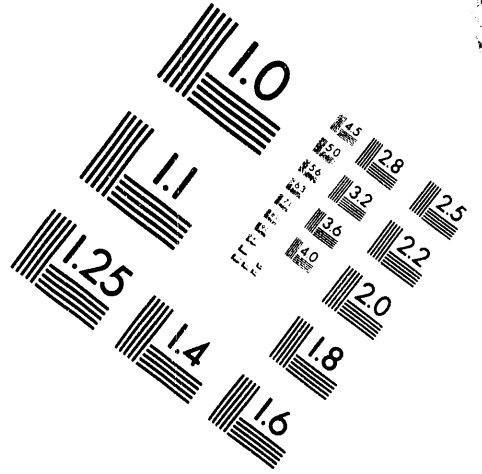
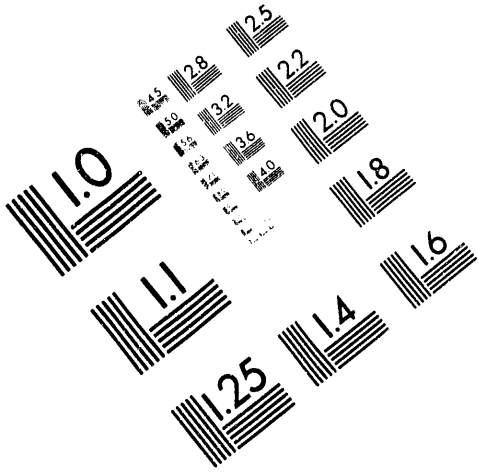




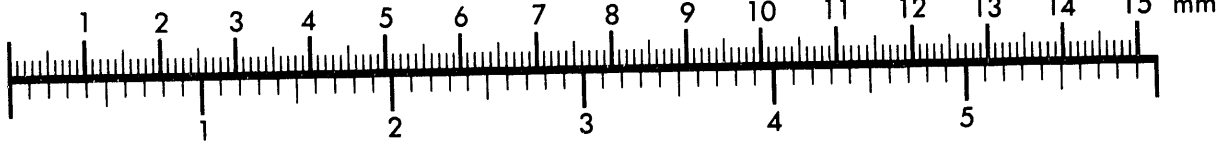
**AIM**

**Association for Information and Image Management**

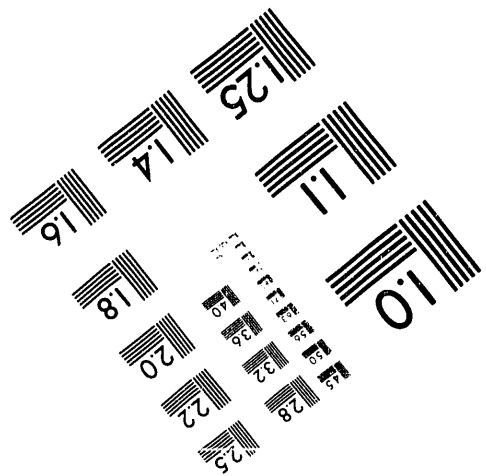
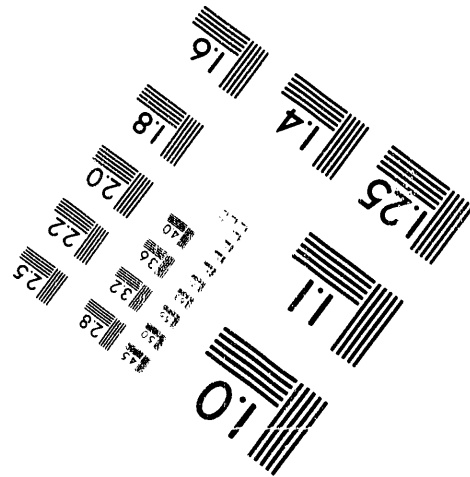
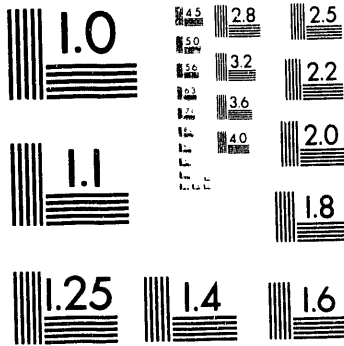
1100 Wayne Avenue, Suite 1100  
Silver Spring, Maryland 20910  
301/587-8202



Centimeter



Inches



MANUFACTURED TO AIM STANDARDS  
BY APPLIED IMAGE, INC.

**1 of 1**

NUMERICAL ANALYSIS OF A THREE-PHASE  
SYSTEM WITH A FLUCTUATING WATER TABLE

**DISCLAIMER**

M. D. White  
R. J. Lenhard

This report was prepared as an account of work sponsored by an agency of the United States Government. Neither the United States Government nor any agency thereof, nor any of their employees, makes any warranty, express or implied, or assumes any legal liability or responsibility for the accuracy, completeness, or usefulness of any information, apparatus, product, or process disclosed, or represents that its use would not infringe privately owned rights. Reference herein to any specific commercial product, process, or service by trade name, trademark, manufacturer, or otherwise does not necessarily constitute or imply its endorsement, recommendation, or favoring by the United States Government or any agency thereof. The views and opinions of authors expressed herein do not necessarily state or reflect those of the United States Government or any agency thereof.

March 1993

Presented at the  
American Geophysical Union  
Hydrology Days  
March 30 - April 2, 1993  
Fort Collins, Colorado

Prepared for  
the U.S. Department of Energy  
under Contract DE-AC06-76RLO 1830

Pacific Northwest Laboratory  
Richland, Washington 99352

**MASTER**

# Numerical Analysis of a Three-Phase System with a Fluctuating Water Table

M. D. White<sup>1</sup> and R. J. Lenhard<sup>1</sup>

## ABSTRACT

Numerical simulations are presented of a one-dimensional, multiphase flow system that involves the redistribution of aqueous-phase liquids and nonaqueous-phase liquids (NAPLs) by a fluctuating water table. The numerical analyses were completed using an integrated-volume, finite-difference-based solution scheme of the governing multiphase conservation equations and constitutive theory. Conservation equations were solved for two components, water and oil, with the assumption of a passive gas-phase. Nonlinearities introduced into the governing conservation equations through the constitutive theory were handled with a multivariable Newton-Raphson iterative scheme. The functional relationships between the phase relative permeability, the phase saturation, and phase pressures in porous media were described with a general theoretical model that includes the effects of air and oil occlusion during imbibition. Parameters required for the theoretical model were defined for two-phase systems (e.g., air-water, air-oil, and oil-water). The theoretical model assumes that wettability decreases in the following order: water, oil, air. Results from the numerical simulations are compared against measurements taken from a previous multiphase flow experiment. The experiment involved subjecting an initially water-drained, three-phase system (i.e., air-oil-water), to a fluctuating water table. The experimental objective was to quantify the entrapment of air and NAPL by phases of greater wettability under dynamic conditions. Comparison of numerical and experimental results were made for two ratios of imbibition to drainage characteristic, curve-shape parameters and two models for relative permeability in two-phase systems. A description of the numerical methods used to solve the governing conservation and constitutive equations for multiphase hysteretic conditions is given.

## INTRODUCTION

The U.S. Department of Energy, through the Office of Technology Development, has requested the demonstration of remediation technologies for the cleanup of volatile organic compounds (VOC) and associated radionuclides within the soil and groundwater at arid sites. A demonstration program, referred to as the VOC-Arid Soils Integrated Demonstration Program (Arid-ID), has been realized that is initially directed at a volume of unsaturated and saturated soil contaminated with carbon tetrachloride on the Hanford Site near Richland, Washington. A critical component of the Arid-ID Program involves the ability to scale laboratory and field experiments to full-scale remediation technologies and to subsequently transfer acquired technologies to other arid sites. Within the Arid-ID Program, proven numerical simulators are recognized as a primary

---

<sup>1</sup> Pacific Northwest Laboratory, P.O. Box 999, Richland, Washington 99352-0999, U.S.A. The laboratory is operated by Battelle Memorial Institute for the U.S. Department of Energy under Contract DE-AC06-76RLO 1830.

mechanism for scaling and transferring remediation technologies. For numerical simulators to predict the behavior of remediation strategies, the soil permeability, saturation, and pressure-characteristic relationships must capture the phenomena of phase distribution and migration. Analyses of previously completed experimental work (Lenhard et al. 1993) suggests that the entrapment of air and nonaqueous liquid phase (NAPL) is required to fully describe phase saturation and relative permeability relations to predict subsurface behavior of three-phase systems (e.g., air-oil-water), where liquid fluctuations occur within the system.

Historically, numerical modelling of multiple-phase fluid flow in porous media has been conducted within the petroleum industry. Because of environmental concerns, as demonstrated by the Arid-ID Program, attention to movement of NAPLs within the vadose and saturated zones has grown. Multiphase flow models directed at organic compound contaminant hydrology that have appeared recently include the numerical models of Falta et al. (1992a; 1992b), Kueper and Frind (1991a; 1991b), Falta et al. (1989), Lenhard et al. (1988), Corapcioglu and Baehr (1987), Baehr (1987), Faust (1985), and Abriola and Pinder (1985). In a review of multiphase flow and transport models for organic compounds, Abriola (1988) recommended that laboratory experiments were needed "to validate the application of immiscible flow models with capillarity to NAPL migration in a variety of scenarios." The numerical modelling described in this paper specifically addresses a multiphase system composed of three immiscible fluids under fluctuating conditions, where the effects of nonwetting fluid entrapment and hysteretic saturation paths are critical to predicting the migration of organic compounds.

This paper describes the theory and application of a multiphase numerical model whose formulation includes capabilities for simulating nonwetting fluid entrapment and hysteretic saturation paths. An emphasis will be placed on the general model formulation and specifics related to the numerical solution scheme for hysteretic saturation paths and phase transitions. Although fully incorporated into the numerical model, only a synopsis of the hysteretic constitutive theory for saturation to pressure and relative permeability to saturation relations will be presented. A complete development of the theory for the hysteretic constitutive relations governing multiphase flow initially appeared in Parker and Lenhard (1987) and Lenhard and Parker (1987). These hysteretic constitutive relations were later refined in Lenhard et al. (1993). A validation exercise of the saturation-pressure component of the relative permeability-saturation-pressure model was reported by Lenhard (1992). Application of the numerical model follows a one-dimensional multiphase flow experiment that was designed to investigate the redistribution of NAPLs in the subsurface as a result of a fluctuating water table (Lenhard et al. 1993). An objective of the experiment was to measure the entrapment of nonwetting fluids under dynamic conditions. Experimental results included water and NAPL water contents, which were measured nondestructively and temporally with a dual-energy gamma-radiation attenuation apparatus. The objective of the application was to compare measured liquid saturations in a transient three-phase experiment with results from numerical simulations based on the hysteretic constitutive theories of Lenhard and Parker. Experimental results will be compared against numerical simulations using two tortuosity or pore interaction models (Burdine 1953; Mualem 1976) for both hysteretic and nonhysteretic saturation paths.

## MULTIPHASE MODEL

The numerical results reported in this paper were generated with a multiphase, subsurface-transport simulator developed specifically to analyze remediation techniques associated with arid sites contaminated with organic compounds and radionuclides (White et al. 1992). The Arid-ID multiphase simulator is formulated to model multiphase subsurface flow and transport of water, air, volatile organic compounds VOC, heat, and radioactive nuclides with three immiscible phases: aqueous, NAPL, and gas. For the subject analysis, the simulator was executed in an operational mode with only two active governing conservation equations. In this operational mode the simulator functions as an isothermal, three-phase, numerical model with a passive gas phase (i.e., no vapor transport). Mathematically, the movement of an aqueous phase and NAPL through porous media was modeled as two-phase flow. By assuming no component partitioning between liquid phases, the conservation equations for water and oil components appear as shown in Equations (1) and (2), where  $\phi$  is the media porosity,  $\rho_w$  and  $\rho_o$  are the water and oil densities,  $s_w$  and  $s_o$  are the actual water and oil saturations,  $\nabla$  is the divergence operator,  $\bar{k}$  is the intrinsic permeability tensor,  $k_{rw}$  and  $k_{ro}$  are the water and oil relative permeabilities,  $\mu_w$  and  $\mu_o$  are the water and oil viscosities,  $P_w$  and  $P_o$  are the water and oil pressures,  $\mathbf{g}$  is the gravitational vector, and  $\dot{m}_w$  and  $\dot{m}_o$  are the liquid-water and liquid-oil source rates.

$$\frac{\partial}{\partial t}(\phi \rho_w s_w) = \nabla \left[ \frac{\bar{k} k_{rw} \rho_w}{\mu_w} (\nabla P_w + \rho_w \mathbf{g}) \right] + \dot{m}_w \quad (1)$$

$$\frac{\partial}{\partial t}(\phi \rho_o s_o) = \nabla \left[ \frac{\bar{k} k_{ro} \rho_o}{\mu_o} (\nabla P_o + \rho_o \mathbf{g}) \right] + \dot{m}_o \quad (2)$$

Closure to the governing conservation equations was provided through the constitutive relations that relate the secondary variables to the primary unknowns. The subject numerical simulator is formulated with the phase pressures as the primary unknowns. Phase densities and viscosities were assumed to be independent of the phase pressures and were fixed during the simulations at values computed for the experimental ambient conditions. The phase saturations and relative permeabilities were related to the phase pressures through the hysteretic constitutive theories of Lenhard and Parker, thus yielding a nonlinear system of partial differential equations.

Lenhard and Parker's constitutive model for saturation-pressure relations does not directly relate actual phase saturations to phase pressures. Instead, apparent saturations are related to scaled pressure-head differences, where apparent saturations include occluded fluids. For example, the apparent water-phase saturation equals the sum of the effective water saturation, plus the occluded oil and air effective saturations. The relationships between apparent total and water saturations and effective saturations are shown in Equations (3) and (4), where  $\bar{s}_w$  and  $\bar{s}_t$  are the apparent water and total saturations,  $\bar{s}_w$  and  $\bar{s}_o$  are the effective water and oil saturations,  $\bar{s}_{at}$  and  $\bar{s}_{ot}$  are the effective trapped air and oil saturations, and  $\bar{s}_{awt}$  is the effective saturation of air occluded by the water phase. A continuous oil phase, which is free to move convectively is referred to as *free oil*, whereas discontinuous islands or ganglia of oil occluded within the water phase and immobile under ambient conditions is referred to as *trapped oil*.

$$\bar{s}_w = \bar{s}_w + \bar{s}_{oi} + \bar{s}_{awi} \quad (3)$$

$$\bar{s}_t = \bar{s}_w + \bar{s}_o + \bar{s}_{ai} \quad (4)$$

The current hysteretic constitutive model assumes that the fluid wettability descends in the following order: water, oil, air. A corollary to this assumption is that only certain two-phase systems are attainable from a three-phase (air-oil-water) system. The two-phase (air-water) system can occur with the disappearance of the oil phase, and the two-phase (oil-water) system can occur when the total saturation equals unity. The two-phase (air-oil) system is assumed unattainable from a system previously containing water. For three-phase (air-oil-water) systems, the total and water apparent saturations are related to the capillary pressure heads according to the expressions shown in Equations (5) and (6), where  $\beta_{ao}$  and  $\beta_{ow}$  are the air-oil and oil-water scaling factors,  $h_{ao}$  and  $h_{ow}$  are the air-oil and oil-water capillary heads, and  $s^*(h^*)$  is the scaled saturation-pressure function. For two-phase (air-water) systems, water apparent saturation is related to the (air-water) capillary pressure head according to the expression shown in Equations (7), where  $\beta_{aw}$  is the air-water scaling factor,  $h_{aw}$  is the air-water capillary head. The air-oil, oil-water, and air-water capillary heads are defined according to Equations (8) through (10), where  $P_a$  is the air pressure and  $g$  is the acceleration of gravity.

$$\bar{s}_t(\beta_{ao} h_{ao}) = s^*(h^*) \quad (5)$$

$$\bar{s}_w(\beta_{ow} h_{ow}) = s^*(h^*) \quad (6)$$

$$\bar{s}_w(\beta_{aw} h_{aw}) = s^*(h^*) \quad (7)$$

$$h_{ao} = \frac{(P_a - P_o)}{g \rho_w} \quad (8)$$

$$h_{ow} = \frac{(P_o - P_w)}{g \rho_w} \quad (9)$$

$$h_{aw} = \frac{(P_a - P_w)}{g \rho_w} \quad (10)$$

For real systems, if no free oil exists (i.e.,  $\bar{s}_t = \bar{s}_w$ ) then two systems are possible. In the first system, no oil exists, and a simple two-phase (air-water) system is indicated. In the second system, only trapped oil exists, and a more subtle system occurs where contaminated air-water interfaces control water saturation. In the presence of trapped oil, a molecular film of organic compound is expected to occur at air-water interfaces resulting in an air-oil / oil-water double meniscus, which controls interface geometry according to Equation (11), where  $\beta'_{aw} = (1/\beta_{ow} + 1/\beta_{ao})^{-1}$  if local phase equilibrium occurs. In the absence of a discrete oil phase, aqueous organic concentrations below the component solubilities will lead to double menisci of less than one monolayer, such that the scaling factor in Equation (11) lies between the saturated value  $\beta_{aw}$

and the value  $\beta_{aw}$ , defined for a system uncontaminated by anthropogenic organics. For numerical stability during phase transitions, an assumption is made in the numerical model that the two-phase scaling factors are related according to Equation (12).

$$\bar{s}_w(\beta'_{aw} h_{aw}) = s^*(h^*) \quad (11)$$

$$\beta_{aw} = \beta'_{aw} = (1/\beta_{ow} + 1/\beta_{ao})^{-1} \quad (12)$$

Van Genuchten's function (1980) was adopted to parameterize the saturation-pressure relationship. Saturation-pressure relationships for the main imbibition and drainage branches are defined according to Equations (13) and (14), where  $i\alpha$ ,  $d\alpha$ , and  $n$  are curve-shape parameters, and  $m = 1 - 1/n$ . The perforatory superscripts  $i$  and  $d$  indicate main imbibition and drainage branches, which refer to increasing or decreasing apparent saturations, respectively. Imbibition and drainage branches other than the main branches are referred to as scanning curves or scanning paths. Saturation-pressure relationships for scanning curves are dependent on the saturation histories. Main branch functions are rescaled to pass through appropriate reversal points, with the constraint of forcing closure on the scanning loops (e.g., an imbibition scanning curve will always return to the previous imbibition to drainage reversal point). This closure constraint requires that a history of nested scanning curves and reversal points be maintained.

$$\begin{aligned} \text{for } h^* \geq 0; \quad i s^*(h^*) &= (1 + (i\alpha h^*)^n)^{-m} \\ \text{for } h^* < 0; \quad i s^*(h^*) &= 1 \end{aligned} \quad (13)$$

$$\begin{aligned} \text{for } h^* \geq 0; \quad d s^*(h^*) &= (1 + (d\alpha h^*)^n)^{-m} \\ \text{for } h^* < 0; \quad d s^*(h^*) &= 1 \end{aligned} \quad (14)$$

Three possible sources of fluid entrapment occur in three-phase (air-oil-water) systems: air trapped by water, air trapped by oil, and oil trapped by water. The amount of nonwetting fluid entrapped by a wetting fluid is dependent on the current fluid saturation and the saturation path. Maximum nonwetting fluid entrapment occurs during wetting along the main imbibition branch. The maximum quantity of trapped nonwetting fluid, for a given saturation reversal from the main drainage branch, is referred to as the effective residual saturation, for a nonwetting and wetting fluid pair. The entrapped nonwetting fluid effective saturation along a primary scanning imbibition path will vary from zero at the main drainage to imbibition reversal point to the effective residual saturation when the apparent saturation of the wetting fluid equals one. The quantity of entrapped, nonwetting fluid is assumed to vary linearly with the apparent saturation of the wetting fluid, in accordance with the assumption that all pores entrap nonwetting fluid proportionately with their volumes, and entrapped nonwetting fluid compressibility is ignored. With respect to nonwetting fluid entrapment, higher order imbibition scanning curves are assumed to follow the same linear dependence with the apparent wetting fluid saturation as their associated primary scanning imbibition path (i.e., higher order imbibition scanning paths are linked to the drainage to wetting reversal point on the main drainage branch).

The hysteretic saturation-pressure relations of the Lenhard and Parker model for three-phase (air-oil-water) systems require ten characteristic parameters:  $d\alpha$ ,  $i\alpha$ ,  $n$ ,  $\beta_{aw}$ ,  $\beta_{ao}$ ,  $\beta_{ow}$ ,  $\bar{s}_{ar}^{aw}$ ,  $\bar{s}_{ar}^{ao}$ ,  $\bar{s}_{or}^{ow}$ ,  $s_m$ . Because the parameters have been defined in terms of two-phase systems, calibration of a three-phase system only requires experimental data from two-phase systems. Parker and Lenhard (1987) proposed two experimental methods for computing the ten characteristic parameters. The first method utilizes measured saturation-capillary pressure head data for primary drainage and imbibition scanning paths from two-phase (air-water, air-oil, and oil-water) systems. The second method requires less experimental effort and utilizes measured saturation-capillary pressure head data for an air-water system drainage. Interfacial tension data is used to estimate scaling coefficients, and relatively simple measurements on two-phase (air-water, air-oil, and oil-water) systems are used to compute effective residual saturations. In the second method, the imbibition curve fitting parameter  $i\alpha$  is estimated as  $i\alpha = 2 d\alpha$  from results reported by Kool and Parker (1987).

Lenhard and Parker (1987) derived closed-form expressions for the permeability-saturation constitutive relations for two- (air-water) and three-phase (air-oil-water) porous media systems for arbitrary saturation paths. For two-phase (air-water) systems, a water relative permeability-saturation expression was derived by modifying Mualem's (1976) model for water relative permeability in two-phase (air-water) systems. Mualem's expression was modified to simultaneously account for the obstruction of water flow and the displacement of water to larger pore spaces by occluded air. The resulting expression shows the water relative permeability for a hysteretic two-phase (air-water) system to be a function of the effective water saturation, the primary imbibition reversal point from main drainage, the effective air residual saturation, and  $m$ , a van Genuchten curve-shape parameter. With respect to the air relative permeability, Mualem's expression was modified to account for the reduction in the free air saturation, which participates in air flow. The air relative permeability was shown to be a function of the same parameters as the water relative permeability.

Using a similar approach to the hysteretic, two-phase (air-water) system, the water relative permeability for a three-phase (air-oil-water) system simultaneously accounts for the obstruction of water flow and the displacement of water to larger pore spaces by water-trapped air and oil. In the three-phase (air-oil-water) system, the water relative permeability was determined to be a function of the current liquid saturations, historical saturations, and the fluid-porous medium parameters. The oil relative permeability relation was derived by accounting for the obstruction of oil flow and the displacement of oil to larger pore spaces by the occluded air. Analogous to the two-phase system, the air relative permeability was derived by substituting the apparent total saturation for the effective total saturation in Mualem's integral expression. Both oil and air relative permeabilities were determined to be a function of the current liquid saturations, historical saturations, and the fluid-porous medium parameters.

Because subsurface contamination scenarios generally include regions with and without NAPL, descriptions of three-phase (air-oil-water) systems must consider the behavior of four saturation regimes: 1) three-phase (air-oil-water) unsaturated, 2) three-phase (air-oil-water) saturated, 3) two-phase (air-

water) unsaturated, and 4) two-phase (air-water) saturated. The following limits were applied in conjunction with Lenhard and Parker's hysteretic constitutive theory to determine the saturation phase condition of the local porous media region. If the scaled air-oil capillary head is less than the scaled oil-water capillary head (i.e.,  $h_{ao} \beta_{ao} < h_{ow} \beta_{ow}$ ), then a three-phase system exists; otherwise a two-phase (air-water) system exists. For three-phase systems, if the air-oil capillary head is greater than zero (i.e.,  $h_{ao} > 0$ ) then unsaturated conditions exist. Analogously for two-phase systems, a positive air-water capillary head (i.e.,  $h_{aw} > 0$ ) indicates unsaturated conditions. The above inequalities were buffered during the application of these saturation phase regime limits in the numerical model to avoid regime flopping during transitions.

## NUMERICAL SOLUTION

The governing partial differential equations were discretized to nonlinear algebraic form using the integrated finite-difference method (Patankar 1980). Transformation of the partial differential equations to algebraic form requires the physical domain be spatially discretized into a computational domain that is composed of a number of nonoverlapping control volumes. Each control volume surrounds a single grid point, which defines the position of intrinsic property variables (e.g., liquid saturation, phase pressure, phase density). The conservation equations are integrated over the control volume by assuming a linear, piecewise profile to express the variation in the primary variables between grid points. The algebraic expressions that result from discretizing the governing conservation equations are nonlinear because of the dependence of liquid saturation and phase relative permeabilities on the primary variables (liquid-phase pressures). The nonlinear algebraic forms of the conservation equations are converted to linear form using a multivariable, residual-based, Newton-Raphson iteration technique (Kreyszig 1979). The technique typically yields quadratic convergence of the residuals with iteration, given sufficiently close initial estimates of the primary variables. Each iteration involves the solution of the linearized algebraic form of the conservation equations. The resulting system of linear equations was solved with a direct, banded-matrix algorithm.

An expression of the multivariable Newton-Raphson technique is shown in Equation (15), where  $\mathbf{R}$  represents the system of nonlinear governing equations expressed in residual form,  $\mathbf{x}$  indicates the vector of unknown variables, and the superscript  $n$  indicates the iteration level. The subject application requires the solution of two governing conservation equations; therefore, the vector of partial derivatives for a particular node  $k$  within the computational domain appears as shown in Equation (16), where  $R_k^w$  and  $R_k^o$  are the discretized forms of the water and oil conservation equations for node  $k$ , respectively, and  $P_{w,l}^n$  and  $P_{o,l}^n$  are the water and oil pressures at iteration level  $n$  and node index  $l$ , respectively. The partial derivatives in Equation (16) were computed numerically following the numerical approximation shown in Equation (17), where  $\Delta P_{w,l}^n$  represents some small increment to the water pressure at iteration level  $n$  and node index  $l$ .

$$\mathbf{x}^{n+1} = \mathbf{x}^n - \frac{\mathbf{R}(\mathbf{x}^n)}{\mathbf{R}'(\mathbf{x}^n)} \quad (15)$$

$$R'_k(x^n) = \frac{\partial R_k}{\partial x^n} = \begin{vmatrix} \frac{\partial R_k^w}{\partial P_{w,l}^n} & \frac{\partial R_k^w}{\partial P_{o,l}^n} \\ \frac{\partial R_k^o}{\partial P_{w,l}^n} & \frac{\partial R_k^o}{\partial P_{o,l}^n} \end{vmatrix} \quad (16)$$

$$\frac{\partial R_k^o}{\partial P_{w,l}^n} \cong \frac{R_k^o(P_{w,l}^n + \Delta P_{w,l}^n) - R_k^o(P_{w,l}^n)}{\Delta P_{w,l}^n} \quad (17)$$

A critical factor in applying the above numerical solution scheme to the solution of the coupled governing conservation equations involves the selection of increments to the primary variables. In the limit, as chosen increments in the primary variables approach zero, the finite difference approximation approaches the analytical partial derivative. A practical limit exists, however, because of precision limitations associated with floating point numbers (i.e., there exist a certain primary variable increment below which the numerator of Equation (17) becomes zero). Primary variables that are excessively large may misrepresent the local partial derivative of the residual function resulting in a nonconvergent iteration scheme. Additional problems exist in choosing primary variable increments when the saturation conditions are near a regime transition. For example, in evaluating the approximation in Equation (17) when the saturation conditions are near a regime boundary, residual function evaluated with an incremented water pressure could be evaluated with hysteretic relations from a different saturation regime than those for the residual function evaluated with a normal water pressure. Using 8-byte, floating-point precision, the rules shown in Table 1 were applied in computing increments to the primary variables.

TABLE 1. Primary Variables Increment Schedule

<u>Water Pressure Increment</u>	<u>Oil Pressure Increment</u>
Saturation Regime: Three-Phase Unsaturated	
$\Delta P_w^* = \max [0.1 \text{ Pa}, 10^{-5} (P_o - P_w)]$	$\Delta P_o^* = \max [0.1 \text{ Pa}, 10^{-5} (P_a - P_o)]$
$\Delta P_w = -\min [10.0 \text{ Pa}, \Delta P_w^*]$	$\Delta P_o = \min [10.0 \text{ Pa}, \Delta P_o^*, (P_a - P_o)]$
Saturation Regime: Three-Phase Saturated	
$\Delta P_w^* = \max [0.1 \text{ Pa}, 10^{-5} (P_o - P_w)]$	$\Delta P_o^* = \max [0.1 \text{ Pa}, 10^{-5} (P_a - P_o)]$
$\Delta P_w = -\min [10.0 \text{ Pa}, \Delta P_w^*]$	$\Delta P_o = \min [10.0 \text{ Pa}, \Delta P_o^*]$
Saturation Regime: Two-Phase Unsaturated	
$\Delta P_w^* = \max [0.1 \text{ Pa}, 10^{-5} (P_a - P_w)]$	$\Delta P_o^* = \max [0.1 \text{ Pa}, 10^{-5} (P_a - P_o)]$
$\Delta P_w = -\min [10.0 \text{ Pa}, \Delta P_w^*]$	$\Delta P_o = \min [10.0 \text{ Pa}, \Delta P_o^*, (P_a - P_o)]$
Saturation Regime: Two-Phase Saturated	
$\Delta P_w^* = \max [0.1 \text{ Pa}, 10^{-5} (P_a - P_w)]$	$\Delta P_o^* = \max [0.1 \text{ Pa}, 10^{-5} (P_a - P_o)]$
$\Delta P_w = -\min [10.0 \text{ Pa}, \Delta P_w^*]$	$\Delta P_o = \min [10.0 \text{ Pa}, \Delta P_o^*]$

## NUMERICAL APPLICATION

The multiphase numerical model described above was applied to a one-dimensional multiphase flow problem, which replicated an experiment designed to investigate the redistribution of NAPLs in the subsurface as a result of a fluctuating water table (Lenhard et al. 1993). The experimental apparatus consisted of a 1-m column, filled to 70 cm with unconsolidated sandy material composed of roughly 97.5, 0.8, 1.7 percent sand-, silt-, and clay-sized particles, respectively. The NAPL was a 1:9 volumetric mixture of 1-iodoheptane and Soltrol-170, a branched alkane solvent manufactured by Phillips Petroleum. The initial condition for the experiment was assumed to be a water-saturated (i.e., no gas entrapment, no NAPL contamination) porous medium with the water table located at the soil surface. At time zero the water table was lowered 5 cm, and then repeatedly lowered 5 cm every 5 min until the water table was 7 cm above the lower soil boundary. The water table remained stationary at 7 cm until 17.4 h. Starting at 12.2 h, 250 ml of NAPL was infiltrated into the soil column over a 46 min period by slightly ponding at the soil surface. NAPL pressure at the soil surface was assumed to be near atmospheric during NAPL infiltration. Starting at 17.4 h, the water table was raised at the rate of 5 cm every 10 min until an elevation of 42 cm was reached. Starting at 19.4 h, the water table was lowered to an elevation of 17 cm at the rate of 5 cm every 10 min, then starting at 21.1 h, the water table was again raised to 52 cm with the same rate of change. Evaporation was minimized from the upper soil boundary, and the upper air-phase boundary condition was atmospheric pressure. Experimental data that included water pressures, NAPL pressures, and water contents were measured at seven vertical elevations. Characteristic parameters for the experiment are listed in Table 2.

TABLE 2. Experimental and Numerical Parameters

<u>Parameter</u>	<u>Symbol</u>	<u>Value</u>
NAPL density	$\rho_o$	830.0 kg/m <sup>3</sup>
NAPL viscosity	$\mu_o$	0.002046 Pa s
Water density	$\rho_w$	998.32 kg/m <sup>3</sup>
Water viscosity	$\mu_w$	0.001023 Pa s
Medium bulk density		1640.0 kg/m <sup>3</sup>
Medium porosity	$\phi$	0.4
Medium hydraulic conductivity		120 cm/hr
van Genuchten curve-shape parameter	$d\alpha$	6.1 1/m
van Genuchten curve-shape parameter	$i\alpha$	9.15 or 12.2 1/m
van Genuchten curve-shape parameter	$n$	3.16
Scaling factor (air-water)	$\beta_{aw}$	1.0
Scaling factor (air-oil)	$\beta_{ao}$	1.8
Scaling factor (oil-water)	$\beta_{ow}$	2.25
Air effective residual saturation (air-water)	$\bar{i}s_{ar}^{aw}$	0.195
Air effective residual saturation (air-oil)	$\bar{i}s_{ar}^{ao}$	0.10
Oil effective residual saturation (oil-water)	$\bar{i}s_{or}^{ow}$	0.35
Minimum residual saturation	$s_m$	0.20

## RESULTS

Numerical and experimental results of NAPL and water saturations are shown in Figures 1 through 9 as a function of time, for three different vertical locations. The experimental results are shown as unconnected symbols, with *open circles* representing the water saturations and *closed circles* representing the NAPL saturations. Numerical results are shown without symbols as lines, where the solid and dashed lines represent results using a slight modification to the Mualem relative permeability model. In the set of simulations referred to as the Mualem model, the tortuosity or pore-interaction term of the Mualem relative permeability was unmodified (i.e.,  $s^{1/2}$ ). In the set of simulations referred to as the Burdine model the tortuosity or pore-interaction term of the Mualem relative permeability was modified (i.e.,  $s^2$ ). NAPL saturations are distinguished from water saturations by noting that NAPL saturations remain zero at least until the onset of NAPL infiltration at 12.12 h. The broken vertical line labeled "NAPL" marks the onset of NAPL infiltration at 12.12 h. The vertical broken lines labeled in sequence "Up", "Down", and "Up" mark the beginning of the water table raising, lowering, and raising at 17.4 h, 19.4 h, and 21.2 h, respectively. Results at the 67-cm point, near the soil surface are shown in Figures 1 through 3, for nonhysteretic constitutive theory and hysteretic constitutive theory with  $i\alpha = 2 d\alpha$  and  $i\alpha = 1.5 d\alpha$ , respectively. Similarly the results at the 37-cm point, mid-way down the column, and at the 17-cm point, near the column bottom, are shown in Figures 4 through 6 and Figures 7 through 9, respectively. To facilitate the discussion of results, model combinations will be referred to with hyphenated names (e.g., the combination of the Mualem relative permeability model and the hysteretic constitutive theory will be referred to as the Mualem-hysteretic model).

The initial segment of the experiment and simulations involve draining the initially water saturated soil column without the presence of oil. Because the drainage process does not entrap air and the van Genuchten curve-shape parameters were experimentally derived from a drainage event, the numerical results show excellent agreement with the experimental results except at the 17-cm point. As expected, no difference between the hysteretic and nonhysteretic constitutive models appear during the initial two-phase (air-water) drainage process. The Mualem relative permeability model generally better predicts the experimental measurements of the water saturation drainage process than does the Burdine model.

At the 67-cm point, the NAPL saturation increases rapidly after the onset of NAPL infiltration because of the proximity to the soil surface, where the NAPL was slightly ponded. The nonhysteretic theory results, Figure 1, predict total saturations equal to 1.0 during the NAPL infiltration period. Although the Mualem relative permeability model predicts higher NAPL saturations than the Burdine model, both relative permeability models in conjunction with the hysteretic theory predict total liquid saturations equal to 0.917, which agrees well with the average total saturation value of 0.92 reported for the experiment during the NAPL infiltration period. This result suggests that air became trapped as NAPL infiltrated. Following the NAPL front, the first water table rise passes unnoticed in all experimental and numerical results except for the Mualem-hysteretic model. The combination of higher relative permeabilities and no fluid entrapment accounts for this result. Because the second water table rise more closely approaches the 67-cm point, increases in both the NAPL and water saturations are noted in both the experimental and numerical results. The

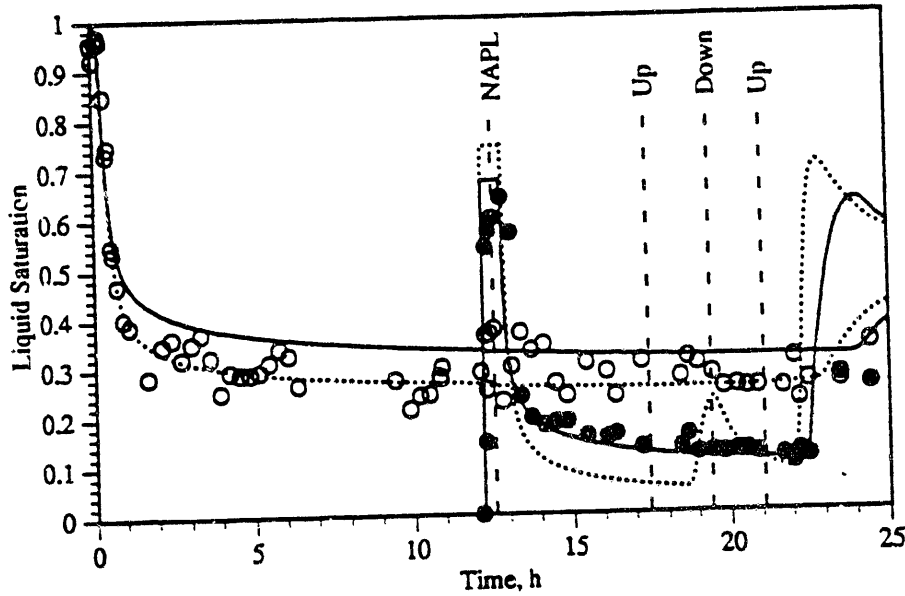


Figure 1. Experimental and Numerical Liquid Saturations (67 cm, Nonhysteretic)

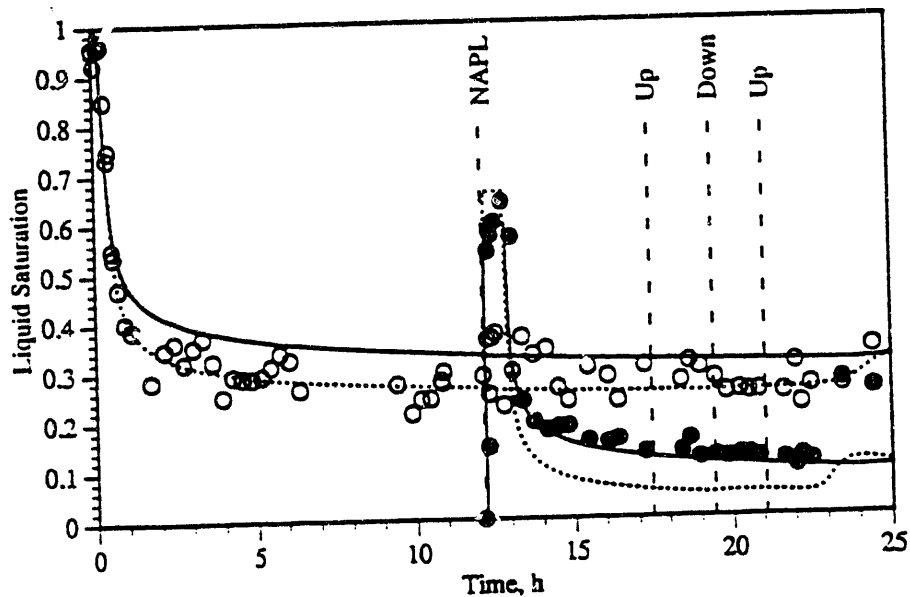


Figure 2. Experimental and Numerical Liquid Saturations (57 cm, Hysteretic with  $\alpha = 2 d\alpha$ )

nonhysteretic simulations notably over predict the saturation increase response demonstrated by the experimental results. The Burdine-hysteretic model shows relatively little response in either the NAPL or water saturation, whereas the Mualem-nonhysteretic model shows a saturation increase response, yet under predicts the change in NAPL saturation demonstrated by the experimental results.

Results at the 37-cm point generally reflect those obtained at the 27-, 47-, and 57-cm points. Appearance of the infiltrated NAPL at the 37-cm point agrees well with the experimental measurements for all numerical modeling

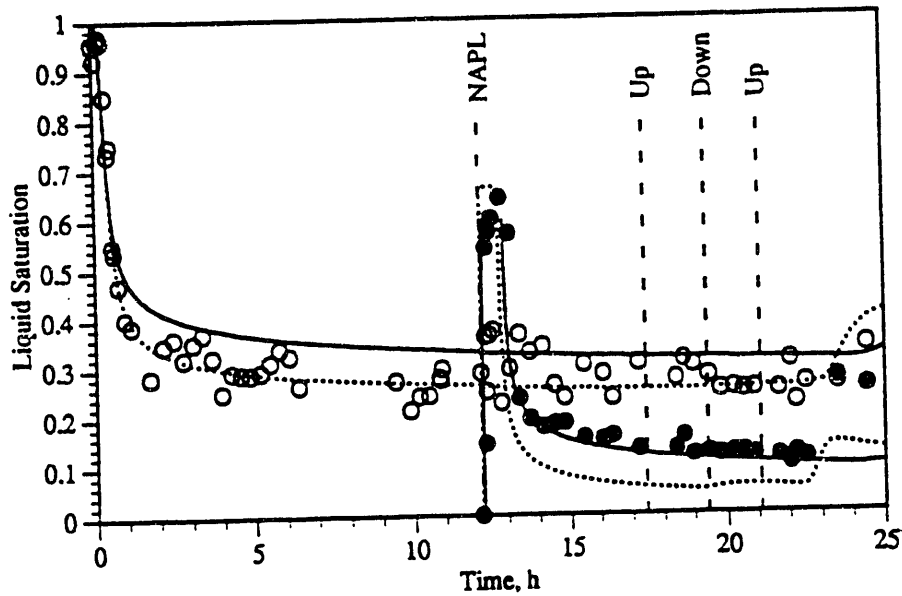


Figure 3. Experimental and Numerical Liquid Saturations  
(67 cm, Hysteretic with  $i\alpha = 1.5 d\alpha$ )

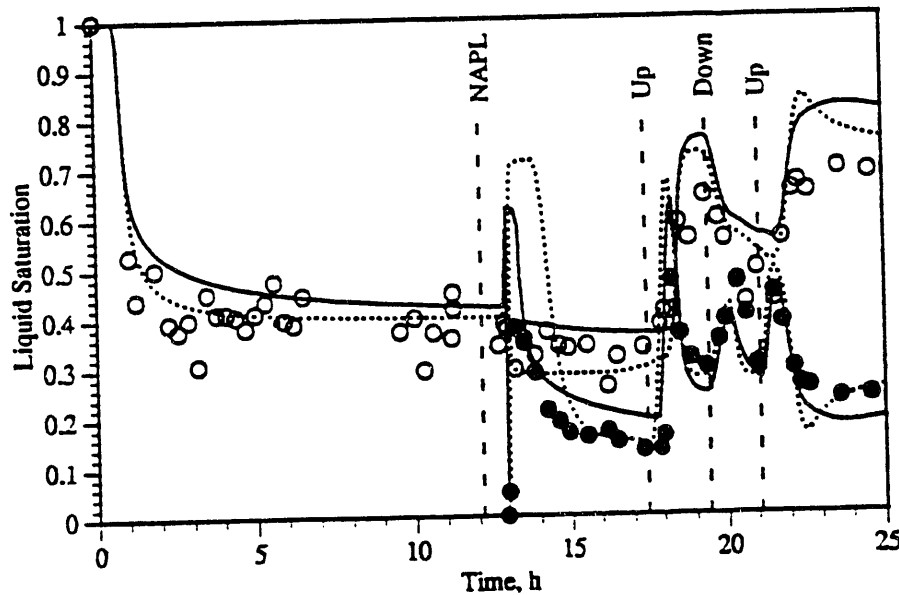


Figure 4. Experimental and Numerical Liquid Saturations  
(37 cm, Nonhysteretic)

schemes. The NAPL saturation response to the descending NAPL front, however, differs significantly among the numerical modeling schemes. As a general observation, the numerical schemes tended to over predict the peak NAPL saturations. The nonhysteretic model showed the worst over predictions of NAPL saturations, whereas the Burdine-hysteretic models, with their lower relative permeabilities, tended to best predict the experimental data. During the peak saturations of the first water table rise, the nonhysteretic constitutive theory predicts total liquid saturations equal to 1.0; whereas the hysteretic models predict total liquid saturations equal to 0.885. Trapped air saturations during

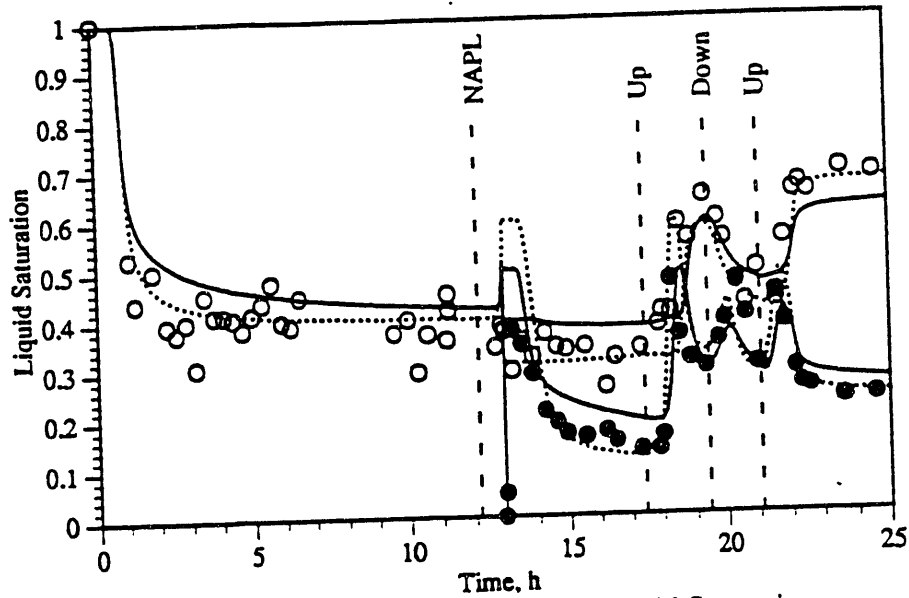


Figure 5. Experimental and Numerical Liquid Saturations  
(37 cm, Hysteretic with  $i\alpha = 2 d\alpha$ )

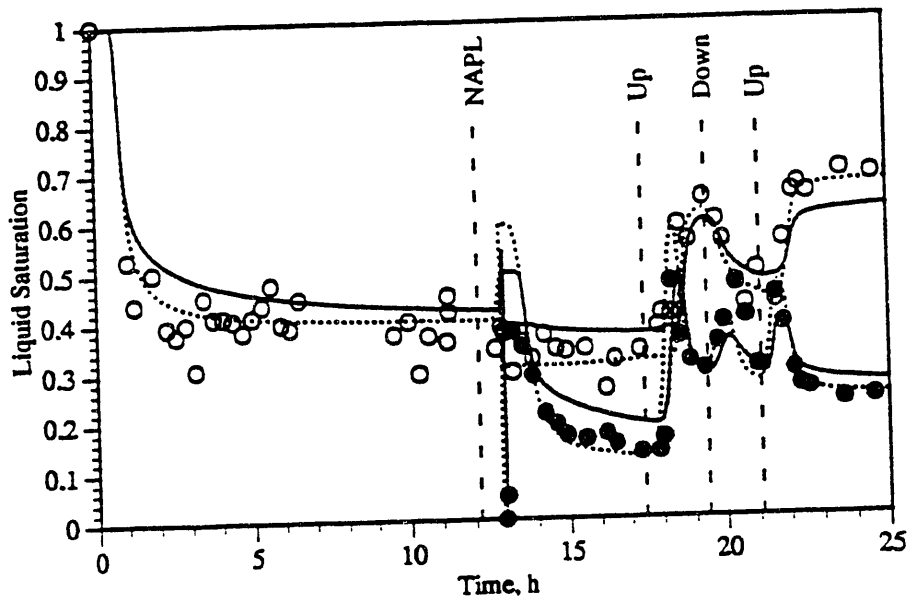


Figure 6. Experimental and Numerical Liquid Saturations  
(37 cm, Hysteretic with  $i\alpha = 1.5 d\alpha$ )

these periods for the hysteretic models equaled 0.115, therefore indicating the water phase was continuous or the porous medium was water saturated. This result agrees with the experimental measurements of fluid pressures at the 37-cm point. An intermediate peak in NAPL saturation occurs between the peaks caused by the water table fluctuations. This peak results from a descending NAPL front passing the 37-cm point in conjunction with the water table lowering sequence. During the second water table rise, the nonhysteretic and hysteretic models predicted total liquid saturations of 1.0 and 0.815, respectively. The experimental results showed a peak total saturation of 0.943 and 0.924 during the first and second water table rises, respectively. Trapped air

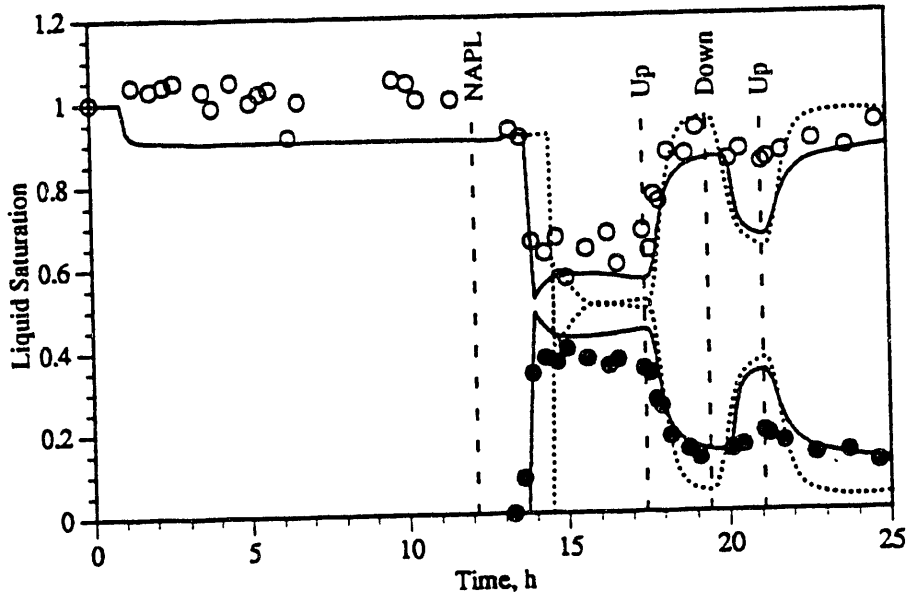


Figure 7. Experimental and Numerical Liquid Saturations  
(17 cm, Nonhysteretic)

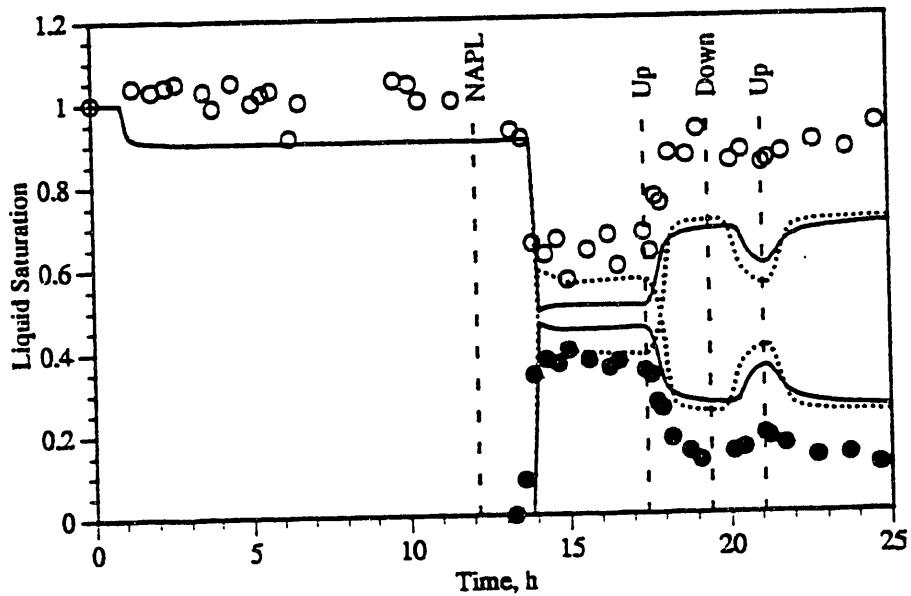


Figure 8. Experimental and Numerical Liquid Saturations  
(17 cm, Hysteretic with  $i\alpha = 2 d\alpha$ )

saturation results for the hysteretic models indicate that contributions to occluded air included air trapped by advancing water-air and oil-air interfaces. Maximum trapped air values, however, are controlled by the effective residual air saturations for oil-air systems.

At the 17-cm point, the porous medium remained liquid saturated throughout the experiments and numerical simulations. In contrast to the other measurement points, the numerical results from the nonhysteretic models show

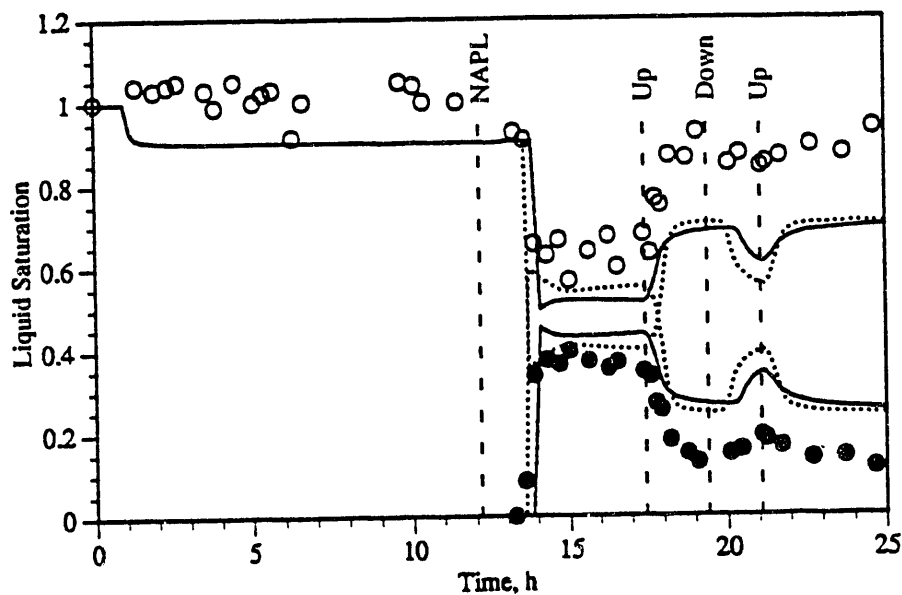


Figure 9. Experimental and Numerical Liquid Saturations  
(17 cm, Hysteretic with  $i\alpha = 1.5 d\alpha$ )

better agreement with the experimental data than do those from the hysteretic models. During the two-phase (air-water) segment of the experiment, measurements of water saturations and pressures suggested that at the 17-cm point the air-entry capillary pressure head was never exceeded. Because the van Genuchten saturation-pressure relationship does not account for a nonwetting fluid entry pressure head, air infiltrates into the water phase at the 17-cm point. In both the experimental and numerical simulations, NAPL infiltrates to the 17-cm elevation prior to the first water table rise. In terms of the experimental results, this suggests that NAPL may infiltrate into regions excluded for air. Again, because of the lack of a model for nonwetting fluid entry head, the numerical simulations allow both air and NAPL infiltration. The equilibrium saturation levels between NAPL and water prior to the first water table rise differ significantly between the constitutive models. For either the hysteretic or nonhysteretic models, the Mualem theory yielded greater NAPL saturations (greater infiltration) than does the Burdine theory, which may be partially due to the greater relative permeabilities predicted by the Mualem model. The hysteretic models yield relatively constant saturation values (0.05) of entrapped air at the 17-cm point after NAPL infiltration. The experimental results do not demonstrate air entrapment by the infiltrating NAPL because air had not displaced water at the 17-cm elevation. As the water table rises during the numerical simulations, the entrapped air is converted from air trapped by oil to air trapped by water as the rising water table displaces oil.

## SUMMARY AND CONCLUSIONS

A numerical method for modeling multiple-phase systems was described and applied to a problem that replicated an experiment designed to measure fluid saturations of a fluctuating three-phase (air-oil-water) system. The numerical theory is appropriate for static or dynamic three-phase (air-oil-water) systems, with provisions for the disappearance of the oil or air phases, where the

wettability of the fluids decreases in the following order: water, oil, air. The objective of the numerical experiment was to compare the hysteretic constitutive theory simulation results against experimental measurements for a three-phase system under dynamic conditions. Variable parameters in the numerical experiment included options for a hysteretic and nonhysteretic constitutive theory, options for either the Burdine or Mualem tortuosity or pore-interaction models for determining phase relative permeabilities, and two ratios of imbibition to drainage curve-shape factors.

With a three-phase (air-oil-water) system, four different phase regimes are possible, with the disappearance of one or two phases. Because the saturation-pressure constitutive theory differs between each of the four phase regimes, discontinuities exist in the gradients of saturation versus capillary pressure across the regime boundaries. These discontinuities, along with a solution scheme based on numerically determined Jacobian matrix coefficients, require special consideration to avoid nonconvergent numerical systems. A numerical solution scheme was presented that successfully models the transition of multiple-phase systems across the regime boundaries. Although successful, the numerical scheme remains somewhat inefficient near regime transitions. Newton-Raphson convergence near these transition regions often shows erratic behavior, dissimilar to the anticipated quadratic convergence.

Comparison of the numerical saturation results with those measured experimentally clearly revealed the inadequacies of a nonhysteretic constitutive theory in describing multiphase porous media flow systems under dynamic conditions. By not accounting for the occlusion of nonwetting fluids and the difference between imbibition and drainage saturation paths, the nonhysteretic numerical results typically show larger responses to field fluctuations than observed experimentally or modeled numerically with the hysteretic models. There was not sufficient evidence from this analysis to categorically state that either the Burdine or Mualem tortuosity or pore-interaction models yielded better comparisons to the experimental data. The Burdine model, however, tended to dampen the system response to fluctuations, probably because of the lower relative permeabilities compared with the Mualem model. The Mualem model appeared considerable more sensitive to transient features of the simulations. Differences between the simulations that used  $i_{\alpha} = 2 d_{\alpha}$  compared with those that used  $i_{\alpha} = 1.5 d_{\alpha}$  were minor, with the latter generally showing closer agreement with the experimental results. The numerical results for the hysteretic constitutive models generally show remarkable agreement with experimental data except at the 17-cm point. Because of the lack of a model for nonwetting fluid entry pressure, infiltrating NAPL was able to entrap air, therefore lowering the actual NAPL saturations. This result suggests a need for a model for nonwetting fluid entry pressure with the hysteretic saturation-pressure relations.

## ACKNOWLEDGEMENT

This research was supported by the VOC-Arid Soils Integrated Demonstration Program, Office of Technology Development and the Subsurface Science Program, Office of Health and Environmental Research of the U.S. Department of Energy. Appreciation is extended to the Subsurface Science Program for providing the scientific basis for the constitutive theory and providing the experimental data for comparison with numerical results.

## REFERENCES

- Abriola, L. M. 1988. *Multiphase Flow and Transport Models for Organic Chemicals: A Review and Assessment* EPRI EA-5976. Electric Power Research Institute, Palo Alto, California. pp. xvii.
- Abriola, L. M. and G. F. Pinder. 1985. "A Multiphase Approach to the Modeling of Porous Media Contamination by Organic Compounds: 1. Equation Development." *Water Resour. Res.* 21(1):11-18.
- Baehr, A. L. 1987. "A Compositional Multiphase Model for Groundwater Contamination by Petroleum Products; 2. Numerical Solution." *Water Resour. Res.* 23(1):201-213.
- Burdine, N. T. 1953. "Relative Permeability Calculations From Pore Size Distribution Data." *Trans. Am. Inst. Min. Metall. Pet. Eng.* 198:71-77.
- Corapcioglu, M. Y. and A. L. Baehr. 1987. "A Compositional Multiphase Model for Groundwater Contamination by Petroleum Products: 1. Theoretical Considerations." *Water Resour. Res.* 23(1):191-200.
- Falta, R. W., I. Javandel, K. Pruess, and P. A. Witherspoon. 1989. "Density-Driven Flow of Gas in the Unsaturated Zone Due to the Evaporation of Volatile Organic Compounds." *Water Resour. Res.* 25(10):2159-2169.
- Falta, R. W., K. Pruess, I. Javandel, and P. A. Witherspoon. 1992a. "Numerical Modeling of Steam Injection for the Removal of Nonaqueous Phase Liquids From the Subsurface: 1. Numerical Formulation." *Water Resour. Res.* 28(2):433-449.
- Falta, R. W., K. Pruess, I. Javandel, and P. A. Witherspoon. 1992b. "Numerical Modeling of Steam Injection for the Removal of Nonaqueous Phase Liquids From the Subsurface: 2. Code Validation and Application." *Water Resour. Res.* 28(2):451-465.
- Faust, C. R. 1985. "Transport of Immiscible Fluids Within and Below the Unsaturated Zone: A Numerical Model." *Water Resour. Res.* 21(4):587-596.
- Kool, J. B., and J. C. Parker. 1987. "Development and Evaluation of Closed-Form Expressions for Hysteretic Soil Hydraulic Properties." *Water Resour. Res.* 23:105-114.
- Kueper, B. H. and E. O. Frind. 1991a. "Two-Phase Flow in Heterogeneous Porous Media: 1. Model Development." *Water Resour. Res.* 27(6):1049-1057.
- Kueper, B. H. and E. O. Frind. 1991b. "Two-Phase Flow in Heterogeneous Porous Media: 2. Model Application." *Water Resour. Res.* 27(6):1059-1070.
- Kreyszig, E. 1979. *Advanced Engineering Mathematics*. 4th ed. John Wiley and Sons, Inc., New York.

- Lenhard, R. J. and J. C. Parker. 1987. "A Model for Hysteretic Constitutive Relations Governing Multiphase Flow: 2. Permeability-Saturation Relations." *Water Resour. Res.* 23(12):2197-2206.
- Lenhard, R. J. 1992. "Measurement and Modeling of Three-Phase Saturation-Pressure Hysteresis." *J. Contaminant Hydrology.* 9:243-269
- Lenhard, R. J., J. H. Dane, J. C. Parker, and J. J. Kaluarachichi. 1988. "Measurement and Simulation of One-Dimensional Transient Three-Phase Flow for Monotonic Liquid Drainage." *Water Resour. Res.* 24(6):853-863.
- Lenhard, R. J., T. G. Johnson, and J. C. Parker. 1993. "Experimental Observations of Nonaqueous-Phase Liquid Subsurface Movement." *Journal of Contaminant Hydrology.* 12(1)
- Mualem, Y. 1976. "A New Model for Predicting the Hydraulic Conductivity of Unsaturated Porous Media." *Water Resour. Res.* 12:513-522.
- Patankar, S. V. 1980. *Numerical Heat Transfer and Fluid Flow.* Hemisphere Publishing Corporation, Washington, D. C.
- Parker, J. C. and R. J. Lenhard. 1987. "A Model for Hysteretic Constitutive Relations Governing Multiphase Flow: 1. Saturation-Pressure Relations." *Water Resour. Res.* 23(12):2187-2196.
- van Genuchten, M. T. 1980. "A Closed-Form Equation for Predicting the Hydraulic Conductivity of Unsaturated Soils." *Soil Sci. Soc. Am. J.* 44:892-898.
- White, M. D., R. J. Lenhard, W. A. Perkins, and K. R. Roberson. 1992. *Arid-ID Engineering Simulator Design Document PNL-8448.* Pacific Northwest Laboratory, Richland, Washington.

**DATE  
FILMED**

8 / 18 / 93

**END**

